PHYSICAL REVIEW B **92**, 041115(R) (2015)

Accurate band gaps of extended systems via efficient vertex corrections in *GW*

Wei Chen* and Alfredo Pasquarello

Chaire de Simulation à l'Echelle Atomique (CSEA), Ecole Polytechnique Fédérale de Lausanne (EPFL), CH-1015 Lausanne, Switzerland

(Received 7 May 2015; published 27 July 2015)

We propose the use of an approximate bootstrap exchange-correlation kernel to account for vertex corrections in self-consistent *GW* calculations. We show that the approximate kernel gives accurate band gaps for a variety of extended systems, including simple *sp* semiconductors, wide band-gap insulators, and transition-metal compounds with either closed or open *d* shells. The accuracy is comparable with that obtained via the solution of the Bethe-Salpeter equation but only at a fraction of the computational cost.

DOI: 10.1103/PhysRevB.92.041115 PACS number(s): 71.10.−w, 71.15.−m

Many-body perturbation theory in Hedin's *GW* approximation is appropriate to describe the electronic band gap [1,2], one of the fundamental properties of semiconductors and insulators. *GW* calculations are often carried out in a perturbative fashion, starting with orbitals and eigenvalues obtained from Kohn-Sham (KS) density functional theory (DFT) [3]. While in general the single-shot G_0W_0 is successful, the accuracy of the calculated band gaps is closely tied to the starting point. For instance, G_0W_0 starting from (semi)local DFT calculations leads to underestimated band gaps, mostly noticeable for wide band-gap materials [4,5]. It eventually fails completely for systems characterized by localized *d* and *f* electrons due to the poor quality of the starting wave functions within the (semi)local approximation [6–8]. The use of hybrid-functional starting points has shown to improve the results [9], but the mixing parameter of Fock exchange needs to be adapted for each material [4].

The dependence of starting point is eliminated through the prescription of self-consistency. Notably, the quasiparticle self-consistent *GW* (QS*GW*) scheme of Faleev, van Schilfgaarde, and Kotani, which casts the *GW* self-energy into a Hermitian model Hamiltonian, gives universally reliable quasiparticle spectra irrespective of the starting point [10,11]. However, it is found that QS*GW* systematically overestimates the band gap by about 20% [4,11,12], as much as the band-gap underestimation found in G_0W_0 calculations with semilocal starting points. The too large band gaps have been ascribed to the missing electron-hole interaction (i.e., the vertex corrections) beyond the random phase approximation (RPA) [13,14], leading to an underestimated dielectric screening in the self-consistent *GW* calculation. In fact, there are pieces of evidence suggesting that vertex corrections have to be included in self-consistent *GW* calculations [14,15]. In particular, when vertex corrections are included in the screening via an effective exchange-correlation kernel $f_{\rm xc}$ (i.e., the NANOQUANTA kernel) derived from the Bethe-Salpeter equation (BSE) [16–20], the QS*GW* scheme has been shown to achieve highly accurate band gaps for a variety of solids [12]. However, such a kernel is computationally too demanding to be applied to extended systems of moderate size.

In this work, we propose the use of an approximate $f_{\rm xc}$ kernel based on the bootstrap procedure [21] to account for the electron-hole interaction in the dielectric screening of the *GW* method. We show that this approximate nonlocal $f_{\rm xc}$ kernel yields accurate band gaps comparable to the full BSE treatment of $f_{\rm xc}$ for a variety of materials, but at a fraction of the computational cost.

We follow the standard *GW* approximation where the self-energy Σ is the product of the one-particle Green's function *G* and the screened Coulomb interaction *W* ($\Sigma = iGW$). The screened interaction is given by $W = \varepsilon^{-1}v$, where ε^{-1} is the microscopic inverse dielectric function, and v the bare Coulomb interaction. For periodic systems, the dielectric matrix (in the basis of reciprocal lattice vectors **G**) can be obtained from the full polarizability χ as

$$\varepsilon^{-1}_{\mathbf{GG'}}(\mathbf{q},\omega) = \delta_{\mathbf{GG'}} + v_{\mathbf{G'}}(\mathbf{q})\chi_{\mathbf{GG'}}(\mathbf{q},\omega). \quad (1)$$

In time-dependent DFT (TDDFT), the full polarizability χ is solved through the Dyson equation

$$\chi = \chi^0 + \chi^0(v + f_{\rm xc})\chi = [1 - \chi^0(v + f_{\rm xc})]^{-1}\chi^0, \quad (2)$$

where χ^0 is the independent-particle polarizability calculated with the one-particle wave functions and eigenvalues. The exchange-correlation kernel is the functional derivative of the exchange-correlation potential with respect to the density:

$$f_{\rm xc}(\mathbf{r},\mathbf{r}',t-t') = \frac{\delta v_{\rm xc}(\mathbf{r},t)}{\delta\rho(\mathbf{r}',t')}. \quad (3)$$

The essential ingredients of the $f_{\rm xc}$ kernel are the nonlocality and the asymptotic long-range behavior $-1/|\mathbf{r}-\mathbf{r}'|$ [16,22]. Various formulations for $f_{\rm xc}$ have been proposed in the context of TDDFT over the years [2]. The NANOQUANTA kernel mapped from the BSE is notably one of the most accurate kernels, but its computational cost can be overwhelming. Simple local approximations, such as the adiabatic local density approximation [23], lack the long-range tail and thereby fail qualitatively to capture the excitonic effect in solids [24]. The long-range contribution (LRC) kernel $f_{\rm xc}^{\rm LRC} = -(a + b\omega^2)/q^2$ is able to predict the excitonic effects of solids via the empirically fitted parameters *a* and *b* [16,25]. However, the extra fitting procedure and, more importantly, the strong material dependence of the parameters restrict the universal application of the LRC kernel.

Here, we adopt the recent bootstrap approximation of $f_{\rm xc}$ [21]. Making use of the exact relationship between $f_{\rm xc}$ and ε^{-1}, the bootstrap method starts with the RPA screening and iterates both quantities via the approximate $f_{\rm xc}$ kernel

*wei.chen@epfl.ch; waynechen@gmail.com

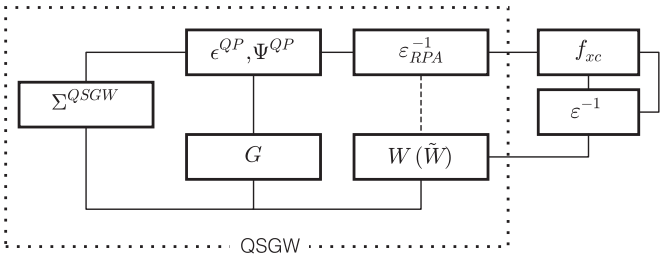

FIG. 1. Diagram sketching the workflow of the present self-consistent QS$G\tilde{W}$ method with the bootstrap $f_{\rm xc}$ included in the screened interaction $\tilde{W}$. The workflow of standard QSGW is shown within the dotted block.

until the convergence is reached. The approximate bootstrap kernel is constructed to satisfy two requirements, namely, the correct behavior in the long-wavelength limit and the dielectric constants in the static limit [21]. The bootstrap $f_{\rm xc}$ kernel [21] can be expressed as

$$f^{\rm boot}_{{\rm xc},\mathbf{GG}'}(\mathbf{q},\omega) = \frac{v^{1/2}_{\mathbf{G}}(\mathbf{q})\varepsilon^{-1}_{\mathbf{GG}'}(\mathbf{q},0)v^{1/2}_{\mathbf{G}'}(\mathbf{q})}{1-\varepsilon^{\rm RPA}_{\mathbf{00}}(\mathbf{q},0)}, \qquad (4)$$

where $\varepsilon^{\rm RPA}$ is the RPA dielectric matrix calculated using Eq. (2) but with vanishing $f_{\rm xc}$. In Eq. (4), we work with the symmetric form of the inverse dielectric function [26]. The $f^{\rm boot}_{\rm xc}$ and ε^{-1} can be determined self-consistently through the iterations of Eqs. (1), (2), and (4). The bootstrap kernel requires no empirical parameters, and it correctly reproduces the long-range behavior $f^{\rm boot}_{\rm xc} \propto 1/q^2$ for $\mathbf{q} \to 0$ as the head (i.e., the $\mathbf{G} = \mathbf{G}' = \mathbf{0}$ component) of χ^0 scales like q^2 in the long-wavelength limit [2]. As the BSE-derived kernel [2], $f^{\rm boot}_{\rm xc}$ is also proportional to the screened interaction. This is intuitive as electron-hole interactions are more prominent in insulators than in semiconductors. In addition, only the static part ($\omega = 0$) is used in the bootstrap kernel. The static approximation is generally adequate and is also often used in BSE calculations [2].

We apply the $f^{\rm boot}_{\rm xc}$ kernel to the self-consistent QSGW method and focus on a variety of materials, ranging from simple sp (Si, SiC, C, AlP, BN, MgO, and LiCl) to transition-metal systems (Ge, GaAs, CdS, ZnO, Cu_2O, and TiO_2). In addition, we consider the antiferromagnetic (AF-II) NiO, a strongly correlated transition-metal oxide with partially filled $3d$ electrons. We implement the kernel in the ABINIT code [27]. Norm-conserving pseudopotentials are used to describe electron-ion interactions. Semicore states are treated explicitly for Li, Mg, Al, and transition metals. Specifically for d-shell elements (e.g., Cd, Cu, Ni, Ga, Ge, and Zn), the semicore sp shells are also treated as valence electrons in the GW calculations [28–30]. The DFT ground-state calculations are performed with the Perdew-Burke-Ernzerhof (PBE)

TABLE I. Band gaps (in eV) calculated at various levels of GW. QS$G\tilde{W}$ includes vertex corrections using the bootstrap kernel in χ. Effects of spin-orbit coupling are accounted for *a posteriori* in the calculated band gaps of GaAs (0.11 eV) and Ge (0.10 eV). For comparison, the QSGW band gaps along with the vertex-corrected ones using the NANOQUANTA kernel reported in Ref. [12] are listed. When available, zero-point renormalization (ZPR) due to electron-phonon couplings is taken into account in the experimental values. Experimental values of the band gaps without ZPR are taken from Ref. [12] if not specified otherwise. The mean absolute error (MAE) is reported with respect to the ZPR-corrected experimental values (TiO_2, NiO, and LiCl are not included in the statistics).

				QSGW		QS$G\tilde{W}$			
	PBE	G_0W_0	QSGW_0	Present	Ref. [12]	Present	Ref. [12]	Expt.+ZPR	Expt.
Si	0.57	1.17	1.28	1.47	1.41	1.30	1.24	1.22[a]	1.17
SiC	1.39	2.25	2.50	2.90	2.88	2.52	2.53	2.51[a]	2.40
C	4.22	5.59	5.85	6.40	6.18	5.90	5.79	5.88[a]	5.48
AlP	1.60	2.49	2.68	3.10	2.90	2.77	2.57	2.47[b]	2.45
Ge	0.00	0.50	0.72	0.96	0.95	0.82	0.81	0.79[b]	0.74
GaAs	0.43	1.10	1.26	1.75	1.84	1.51	1.61	1.55[c]	1.52
CdS	1.21	2.31	2.59	3.41	2.87	2.74	2.39	2.48[b]	2.42
ZnO	0.85	2.28	3.17	4.61	3.8	3.42	3.2	3.60[b]	3.44
Cu_2O	0.53	1.36	1.70	2.65		2.12		2.20[b]	2.17[d]
TiO_2	1.90	3.32	3.37	4.22		3.73			3.3[e]
NiO	1.05	1.74	2.45	4.97		4.40			4.3[f]
BN	4.53	6.19	6.65	7.51	7.14	6.67	6.59	6.6[g]	6.3
MgO	4.68	7.08	7.89	9.29	9.16	8.30	8.12	7.98[g]	7.83
LiCl	6.52	9.27	9.80	10.98		9.87			9.4[h]
MAE	1.57	0.45	0.17	0.62	0.40	0.13	0.10		

[a]Zero-point renormalization taken from Ref. [34] (Si: 0.05 eV; SiC: 0.11 eV; C: 0.40 eV).
[b]Zero-point renormalization taken from Ref. [35] (AlP: 0.02 eV; Ge: 0.05 eV; CdS: 0.06 eV; ZnO: 0.16 eV; Cu_2O: 0.03 eV).
[c]Zero-point renormalization for GaAs (0.03 eV) from Ref. [36].
[d]Reference [37].
[e]Reference [38].
[f]Reference [39].
[g]Zero-point renormalization taken from Ref. [40] (BN: 0.26 eV; MgO: 0.15 eV).
[h]Reference [41].

exchange-correlation functional [31]. Experimental lattice parameters are used throughout. A $6 \times 6 \times 6$ Monkhorst-Pack **k**-point mesh [32] is generally used except for Cu_2O ($5 \times 5 \times 5$), ZnO ($6 \times 6 \times 4$), rutile TiO_2 ($5 \times 5 \times 7$), and NiO ($8 \times 8 \times 4$). Single-shot G_0W_0 calculations use the DFT-PBE wave functions and eigenvalues as starting point. In self-consistent GW calculations, both wave functions and quasiparticle energies are iterated to convergence. The frequency dependence in the dielectric matrices $\varepsilon^{-1}(\omega)$ is evaluated by the contour deformation method [33]. A plane-wave energy cutoff of 25 Ry is used to include the local field effect. A sufficiently large number of unoccupied bands (typically 500 to 1000) are included in the present GW calculations to ensure the convergence of the quasiparticle energies.

To distinguish the current implementation of $f_{\rm xc}^{\rm boot}$ from the standard QSGW in the RPA ($f_{\rm xc} = 0$), we denote our method as QS$G\tilde{W}$. The workflow of QS$G\tilde{W}$ is sketched in Fig. 1, showing a small addition to the original QSGW scheme with the new $f_{\rm xc}$ loop. We also consider the QSGW_0 scheme in which the screened interaction is fixed at the PBE level (W_0) [4]. Band gaps of semiconductors and insulators calculated at various levels of GW are presented in Table I. Note that the comparison with experimental band gaps can be complicated by the fact that the electron-phonon coupling, which effectively reduces the band gap even at zero temperature, has not been included in the present theoretical framework. The zero-point renormalization (ZPR) can be sizable, for example, of the order of half an electronvolt in the case of diamond [34,36,42]. When available, to facilitate a direct comparison, Table I also reports revised experimental band gaps that have been corrected for the ZPR. In Fig. 2, the calculated band gaps are plotted against the (ZPR corrected) experimental values.

From Table I and Fig. 2, it is clear that some well-known results are recovered. The single-shot G_0W_0 on top of the PBE starting point generally gives underestimated band gaps, whereas the full self-consistent QSGW significantly overshoots the band gaps for all materials by a mean absolute error (MAE) of 0.6 eV. The QSGW_0 method performs generally well, but the band gaps remain too small for transition-metal compounds (e.g., for GaAs, ZnO, Cu_2O, and NiO), mostly as a result of the overestimated screening obtained at the PBE level [12]. By contrast, the inclusion of $f_{\rm xc}^{\rm boot}$ in QS$G\tilde{W}$ successfully corrects the underscreening in QSGW, reconciling the calculated band gaps with the experimental ones consistently across the set of considered materials, as manifested by the MAE of 0.1 eV. This also applies to the strongly correlated NiO, which is notoriously difficult to describe in electronic-structure methods [10,43,44].

The agreement is generally improved when the experimental band gaps are corrected for the zero-point electron-phonon renormalization. In particular, it is noteworthy that QS$G\tilde{W}$ accurately reproduces the band gaps of the $3d$ transition-metal systems. For LiCl, the remaining overestimation is expected to be due to electron-phonon coupling and possibly to the effect of lattice polarization [45,46] which are not accounted for here. Likewise, the overestimated band gap (3.7 eV) of rutile TiO_2 can be rationalized in light of the large contribution from phonons [47–49]. Furthermore, we find that the band-gap renormalization (i.e., referred to QSGW results) obtained here with $f_{\rm xc}^{\rm boot}$ closely corresponds to that obtained with the NANOQUANTA kernel in Ref. [12] (cf. Table I). The good agreement indicates that the simple $f_{\rm xc}^{\rm boot}$ kernel is indeed adequate to account for vertex corrections in the screening.

We note that the band gap of ZnO is known to be an extremely difficult case [50–52]. The present calculations use about 1000 bands for ZnO, giving rise to a G_0W_0 band gap of 2.28 eV in good agreement with the carefully converged result (2.35 eV) obtained in Ref. [51] with norm-conserving pseudopotentials. However, we note that recent all-electron calculations yield a larger G_0W_0 band gap of 2.8 eV [5,52]. The origin of the difference between the norm-conserving and all-electron results is not yet fully understood. Nevertheless, we remark that the band gap of 3.42 eV obtained with the present self-consistent QS$G\tilde{W}$ scheme shows a rather good agreement with the ZPR-corrected experimental band gap of 3.60 eV.

Apart from the band gap, the precise positioning of band-edge states is also relevant, for example, in calculations involving defect energy levels [53,54] and band alignments [55]. Band-edge positions cannot be extracted directly from periodic bulk calculations, but their accuracy can be examined by ionization potentials (IPs) calculated through the use of surface slabs [4,56,57]. We obtain the IPs by combining GW quasiparticle corrections of the bulk VBM with the electrostatic potential alignment across the surface determined at the PBE level. The PBE alignment agrees well with higher levels of theory, namely, hybrid functionals [58,59] and GW [55], and

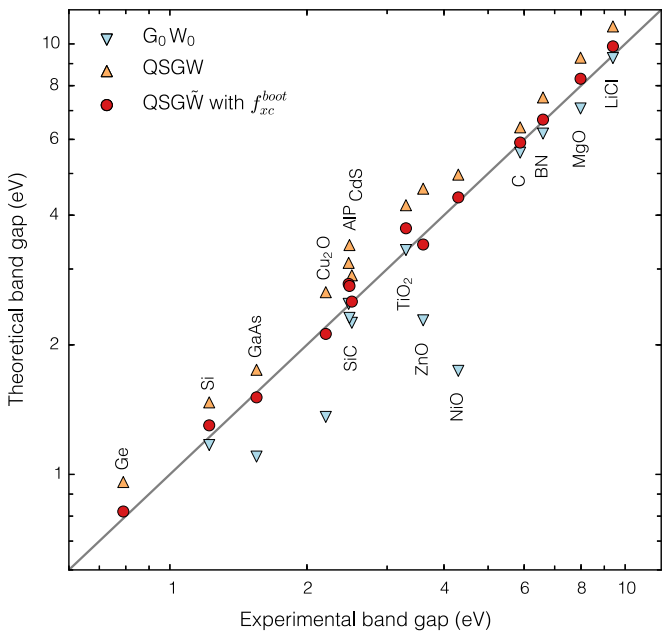

FIG. 2. (Color online) Theoretical (G_0W_0, QSGW, and QS$G\tilde{W}$) vs experimental band gaps plotted on a logarithmic scale. Points in closer vicinity of the diagonal line show better agreement with experiment. Zero-point electron-phonon renormalization is taken into account in the experimental values except for rutile TiO_2, NiO, and LiCl.

TABLE II. Calculated ionization potentials (in eV) of various surfaces, including Si(111), C(111), GaAs(110), ZnO($10\bar{1}0$), TiO_2(110), and MgO(100). The calculated ionization potentials of GaAs are corrected for spin-orbit coupling. Experimental values are taken from Refs. [4,57].

	PBE	G_0W_0	QSGW	QS$G\tilde{W}$	$G_0\tilde{W}_0(\alpha)$	Expt.
Si	4.81	5.47	5.71	5.72	5.53	5.15, 5.35
C	5.59	6.50	6.94	6.87	6.52	5.85, 6.00, 6.5
GaAs	4.60	5.20	5.55	5.52	5.43	5.47, 5.56
ZnO	5.95	7.17	8.80	8.24	7.70	7.82
TiO_2	7.26	7.66	8.64	8.46	8.15	8.0, 8.2
MgO	5.18	6.84	8.33	8.10	7.43	7.15

is commonly used for the determination of IPs [56,57,60]. Details of the slab calculations, e.g., the number of slabs and the **k**-point samplings, are the same as described in Ref. [4]. The calculated IPs for a selection of semiconductor and oxide surfaces are shown in Table II. Overall, QS$G\tilde{W}$ outperforms G_0W_0 and QSGW in terms of accuracy of calculated IPs. However, the comparison with experimental IPs shows that the calculated IPs are generally too large. This could possibly be due to the systematic overestimation of the band gaps in QS$G\tilde{W}$.

To examine effects arising from errors in the estimation of the band gap, we consider an alternative scheme, denoted as $G_0\tilde{W}_0(\alpha)$ in Table II. In this scheme, we calculate the IP while ensuring that the calculated band gap matches the experimental one. Instead of being self-consistent, the perturbative $G_0\tilde{W}_0(\alpha)$ scheme makes use of a hybrid-functional starting point (PBE0 [61]) so that one can achieve the experimental band gap by empirically adjusting the fraction α of Fock exchange in the hybrid functional. As in QS$G\tilde{W}$, the $f_{\rm xc}^{\rm boot}$ kernel is included in the screening of $G_0\tilde{W}_0(\alpha)$. As seen in Table II, this scheme leads to IPs systematically in better agreement with experiment. Note that the IPs are still slightly overestimated for semiconductors such as Si and diamond. Recently, Grüneis *et al.* suggested that further improvement of the IPs could be achieved via the proper inclusion of vertex corrections in the self-energy [57]. On the other hand, vertex corrections in the self-energy have a very limited effect on the band gap, typically enlarging the band gap by less than 0.1 eV [57]. As far as the band gap is concerned, the inclusion of vertex corrections in the screening alone is thus adequate.

In conclusion, we have demonstrated the efficient inclusion of vertex corrections in the screening of GW calculations via the bootstrap approximation of the exchange-correlation kernel. Combined with quasiparticle self-consistent GW, this leads to accurate band gaps for a variety of semiconductors and insulators without the use of any adjustable parameters. Remarkably, we show that the band gaps of various transition-metal compounds can be well reproduced. The present implementation of vertex corrections costs roughly the same as standard self-consistent GW calculations, making the method particularly useful for band-gap predictions of large-scale systems.

We thank G.-M. Rignanese for illuminating discussions on exchange-correlation kernels. Financial support is acknowledged from the Swiss National Science Foundation (SNSF) under Grants No. 200020-134600 and No. 200020-152799. This work has been realized in relation to the National Center of Competence in Research (NCCR) "Materials' Revolution: Computational Design and Discovery of Novel Materials (MARVEL)" of the SNSF. We used computational resources of CSCS and CSEA-EPFL.

[1] L. Hedin, Phys. Rev. **139**, A796 (1965).
[2] G. Onida, L. Reining, and A. Rubio, Rev. Mod. Phys. **74**, 601 (2002).
[3] M. S. Hybertsen and S. G. Louie, Phys. Rev. B **34**, 5390 (1986).
[4] W. Chen and A. Pasquarello, Phys. Rev. B **90**, 165133 (2014).
[5] J. Klimeš, M. Kaltak, and G. Kresse, Phys. Rev. B **90**, 075125 (2014).
[6] F. Bruneval, N. Vast, L. Reining, M. Izquierdo, F. Sirotti, and N. Barrett, Phys. Rev. Lett. **97**, 267601 (2006).
[7] M. Gatti, F. Bruneval, V. Olevano, and L. Reining, Phys. Rev. Lett. **99**, 266402 (2007).
[8] J. Vidal, F. Trani, F. Bruneval, M. A. L. Marques, and S. Botti, Phys. Rev. Lett. **104**, 136401 (2010).
[9] F. Fuchs, J. Furthmüller, F. Bechstedt, M. Shishkin, and G. Kresse, Phys. Rev. B **76**, 115109 (2007).
[10] S. V. Faleev, M. van Schilfgaarde, and T. Kotani, Phys. Rev. Lett. **93**, 126406 (2004).
[11] M. van Schilfgaarde, T. Kotani, and S. Faleev, Phys. Rev. Lett. **96**, 226402 (2006).
[12] M. Shishkin, M. Marsman, and G. Kresse, Phys. Rev. Lett. **99**, 246403 (2007).
[13] R. Del Sole, L. Reining, and R. W. Godby, Phys. Rev. B **49**, 8024 (1994).
[14] F. Bechstedt, K. Tenelsen, B. Adolph, and R. Del Sole, Phys. Rev. Lett. **78**, 1528 (1997).
[15] E. L. Shirley, Phys. Rev. B **54**, 7758 (1996).
[16] L. Reining, V. Olevano, A. Rubio, and G. Onida, Phys. Rev. Lett. **88**, 066404 (2002).
[17] F. Sottile, V. Olevano, and L. Reining, Phys. Rev. Lett. **91**, 056402 (2003).
[18] G. Adragna, R. Del Sole, and A. Marini, Phys. Rev. B **68**, 165108 (2003).
[19] A. Marini, R. Del Sole, and A. Rubio, Phys. Rev. Lett. **91**, 256402 (2003).
[20] F. Bruneval, F. Sottile, V. Olevano, R. Del Sole, and L. Reining, Phys. Rev. Lett. **94**, 186402 (2005).
[21] S. Sharma, J. K. Dewhurst, A. Sanna, and E. K. U. Gross, Phys. Rev. Lett. **107**, 186401 (2011).
[22] P. Ghosez, X. Gonze, and R. W. Godby, Phys. Rev. B **56**, 12811 (1997).
[23] M. A. Marques, N. T. Maitra, F. M. Nogueira, E. K. Gross, and A. Rubio, *Fundamentals of Time-Dependent Density Functional Theory* (Springer, Berlin, 2012), Vol. 837.

[24] V. I. Gavrilenko and F. Bechstedt, Phys. Rev. B **55**, 4343 (1997).
[25] S. Botti, A. Fourreau, F. Nguyen, Y.-O. Renault, F. Sottile, and L. Reining, Phys. Rev. B **72**, 125203 (2005).
[26] P. B. Allen, M. L. Cohen, and D. R. Penn, Phys. Rev. B **38**, 2513 (1988).
[27] X. Gonze, B. Amadon, P.-M. Anglade, J.-M. Beuken, F. Bottin, P. Boulanger, F. Bruneval, D. Caliste, R. Caracas, M. Côté, T. Deutsch, L. Genovese, P. Ghosez, M. Giantomassi, S. Goedecker, D. Hamann, P. Hermet, F. Jollet, G. Jomard, S. Leroux, M. Mancini, S. Mazevet, M. Oliveira, G. Onida, Y. Pouillon, T. Rangel, G.-M. Rignanese, D. Sangalli, R. Shaltaf, M. Torrent, M. Verstraete, G. Zerah, and J. Zwanziger, Comput. Phys. Commun. **180**, 2582 (2009).
[28] M. Rohlfing, P. Krüger, and J. Pollmann, Phys. Rev. Lett. **75**, 3489 (1995).
[29] W. Luo, S. Ismail-Beigi, M. L. Cohen, and S. G. Louie, Phys. Rev. B **66**, 195215 (2002).
[30] M. L. Tiago, S. Ismail-Beigi, and S. G. Louie, Phys. Rev. B **69**, 125212 (2004).
[31] J. P. Perdew, K. Burke, and M. Ernzerhof, Phys. Rev. Lett. **77**, 3865 (1996).
[32] H. J. Monkhorst and J. D. Pack, Phys. Rev. B **13**, 5188 (1976).
[33] S. Lebègue, B. Arnaud, M. Alouani, and P. E. Bloechl, Phys. Rev. B **67**, 155208 (2003).
[34] B. Monserrat and R. J. Needs, Phys. Rev. B **89**, 214304 (2014).
[35] M. Cardona and M. L. W. Thewalt, Rev. Mod. Phys. **77**, 1173 (2005).
[36] G. Antonius, S. Poncé, P. Boulanger, M. Côté, and X. Gonze, Phys. Rev. Lett. **112**, 215501 (2014).
[37] P. W. Baumeister, Phys. Rev. **121**, 359 (1961).
[38] Y. Tezuka, S. Shin, T. Ishii, T. Ejima, S. Suzuki, and S. Sato, J. Phys. Soc. Jpn. **63**, 347 (1994).
[39] G. A. Sawatzky and J. W. Allen, Phys. Rev. Lett. **53**, 2339 (1984).
[40] G. Antonius, S. Poncé, É. Lantagne-Hurtubise, G. Auclair, X. Gonze, and M. Côté, arXiv:1505.07738.
[41] G. Baldini and B. Bosacchi, Phys. Status Solidi B **38**, 325 (1970).
[42] F. Giustino, S. G. Louie, and M. L. Cohen, Phys. Rev. Lett. **105**, 265501 (2010).
[43] C. Rödl, F. Fuchs, J. Furthmüller, and F. Bechstedt, Phys. Rev. B **79**, 235114 (2009).
[44] H. Jiang, R. I. Gomez-Abal, P. Rinke, and M. Scheffler, Phys. Rev. B **82**, 045108 (2010).
[45] F. Bechstedt, K. Seino, P. H. Hahn, and W. G. Schmidt, Phys. Rev. B **72**, 245114 (2005).
[46] S. Botti and M. A. L. Marques, Phys. Rev. Lett. **110**, 226404 (2013).
[47] C. Persson and A. Ferreira da Silva, Appl. Phys. Lett. **86**, 231912 (2005).
[48] W. Kang and M. S. Hybertsen, Phys. Rev. B **82**, 085203 (2010).
[49] L. Chiodo, J. M. García-Lastra, A. Iacomino, S. Ossicini, J. Zhao, H. Petek, and A. Rubio, Phys. Rev. B **82**, 045207 (2010).
[50] B.-C. Shih, Y. Xue, P. Zhang, M. L. Cohen, and S. G. Louie, Phys. Rev. Lett. **105**, 146401 (2010).
[51] M. Stankovski, G. Antonius, D. Waroquiers, A. Miglio, H. Dixit, K. Sankaran, M. Giantomassi, X. Gonze, M. Côté, and G.-M. Rignanese, Phys. Rev. B **84**, 241201 (2011).
[52] C. Friedrich, M. C. Müller, and S. Blügel, Phys. Rev. B **83**, 081101 (2011).
[53] W. Chen and A. Pasquarello, Phys. Rev. B **88**, 115104 (2013).
[54] W. Chen and A. Pasquarello, J. Phys.: Condens. Matter **27**, 133202 (2015).
[55] R. Shaltaf, G.-M. Rignanese, X. Gonze, F. Giustino, and A. Pasquarello, Phys. Rev. Lett. **100**, 186401 (2008).
[56] H. Jiang and Y.-C. Shen, J. Chem. Phys. **139**, 164114 (2013).
[57] A. Grüneis, G. Kresse, Y. Hinuma, and F. Oba, Phys. Rev. Lett. **112**, 096401 (2014).
[58] A. Alkauskas, P. Broqvist, F. Devynck, and A. Pasquarello, Phys. Rev. Lett. **101**, 106802 (2008).
[59] K. Steiner, W. Chen, and A. Pasquarello, Phys. Rev. B **89**, 205309 (2014).
[60] T. A. Pham, C. Zhang, E. Schwegler, and G. Galli, Phys. Rev. B **89**, 060202 (2014).
[61] J. P. Perdew, M. Ernzerhof, and K. Burke, J. Chem. Phys. **105**, 9982 (1996).